www.czasopisma.pan.pl PAN POLSKA AKADEMIA NAUK www.journals.pan.pl

PAN ARCHIVES OF ACOUSTICS
Vol. **45**, No. 4, pp. 709–720 (2020)
DOI: 10.24425/aoa.2020.135277

Research Paper

Impact of Spatial Noise Correlation on Bearing Accuracy in DIFAR Systems

Mariusz RUDNICKI*, Jacek MARSZAL, Roman SALAMON

Gdansk University of Technology
Faculty of Electronics, Telecommunications and Informatics
Department of Sonar Systems
Gdansk, Poland
*Corresponding Author e-mail: mariusz.rudnicki@pg.edu.pl

(*received July 5, 2020; accepted September 24, 2020*)

DIFAR type underwater passive systems are one of the more commonly used tools for detecting submarines. At the design stage, which usually uses computer simulations, it is necessary to generate acoustic noise of the sea. It has been shown that correlating noise significantly reduces these errors compared to the assumption that noise is uncorrelated. In addition, bearing errors have been shown to be the same in systems with a commonly used antenna containing five hydrophones, as in a system without a central hydrophone, which may be useful in some DIFAR system design solutions.

Keywords: underwater noise, noise correlation, DIFAR sonobuoys, bearing accuracy.

1. Introduction

One of the most commonly used means of detection and location of submarines is the Directional Frequency Analysis and Recording (DIFAR) sonobuoys system. This is a passive system that operates by receiving the acoustic signals emitted by submarines, detecting them and locating them. In recent years, DIFAR sonobuoys have also been used to track the migrations of whales and to record the sounds they emit (McDonald, 2004; Miller, 2012; Greene Jr. *et al.*, 2004). In general, DIFAR sonobuoys are equipped with a hydroacoustic antenna consisting of five hydrophones, which constitute crossed pairs of gradient hydrophones and an additional central hydrophone (Mallet, 1975; Salamon, 2004). Similar antenna systems without a central hydrophone are also known (Stover, 1969; Salamon *et al.*, 2000). In this paper, the authors will prove that both solutions are correct and provide similar bearing accuracy levels across a wide range of signal-to-noise ratios.

As in any passive or active acoustic system, bearing accuracy is influenced by noise, of which the level in the operating frequency range of sonobuoys (10 Hz to 3 kHz) is particularly high (Salamon, 2004; 2006; Marszal *et al.*, 2005). The knowledge of the impact of noise on bearing accuracy is thus essential at the system design stage. Although the knowledge of the acoustic noise of the oceans and seas (also regarding the shallow Baltic Sea) is very rich (Salamon, 2006; Urick, 1983; 1986; Burdick, 1984; Marage, Mori, 2010; Klusek, 2011; Klusek, Lisimenka, 2016; Kozaczka, Grelowska, 2011; Grelowska *et al.*, 2013; Rudnicki, MarszAl, 2016), underwater acoustic systems, in particular the DIFAR system, also require – as shown below – knowledge of their spatial correlation level.

Theoretical and experimental research on the correlation of acoustic noise in the sea has been conducted for decades (Cron, Sherman, 1962; Cox, 1973) and has covered increasingly extensive aspects of this question. Most theoretical papers are based on analytical noise and acoustic wave propagation models using the Green's functions (Roux *et al.*, 2005; Buckingham, 2011). They determine the correlation function, the cross-correlation density function or correlation coefficients (Ren, Huang, 2020). Surface noise sources (wave noise), isotropic noise (Ren, Huang, 2020; Buckingham, 2012) and vector noise fields (Zhou *et al.*, 2017) have also been analysed. In (Buckingham, 2011), noise sources are placed on the surface of spheres and their specimens, which is close

to the noise model proposed in this paper. Noise propagation also includes absorption attenuation and refraction caused by the depth distribution of the speed of sound in oceans. The impact of noise filtering on the correlations is analysed as well (Buckingham, 2012). The research covers noise correlation for hydrophones arranged on the horizontal planes or vertically (Cox 1973; Buckingham, 2011; 2012; Ren, Huang, 2020; Zhou *et al.*, 2017; Yang *et al.*, 2018).

In order to investigate the impact of the shape of sound speed profiles on the vertical noise-correlation, in the case of the surface-generated noise, experimental research were conducted in deep ocean waters (Barclay, Buckingham, 2014; 2016).

The above-quoted and other publications provide broad and detailed knowledge of acoustic noise correlation in the sea, which is valuable during the operation of active and, in particular, passive underwater acoustic systems. Based on a computer simulation, which is the common design stage at present, developing a numerical model of spatially-correlated noise seems useful. This is one of the objectives of this paper. Another objective is to investigate the impact of noise correlation on bearing errors in the DIFAR system. A developed numerical model of correlated noise was used for this purpose.

The developed numerical model of spatial noise correlation of the site can also be used in the design of other sonar systems with multi-transducer antennas, and hydroacoustic underwater communication systems (Kochańska *et al.*, 2018; Schmidt *et al.*, 2018).

2. Operating principle of the system

In most DIFAR type systems, the acoustic part consists of five hydrophones (H0, H1, H2, H3, and H4) placed in the horizontal plane, as shown in Fig. 1. The hydrophones are usually piston piezoelectric transducers with a circular surface (Mallet, 1975; Salamon, 2004; Stover, 1969) and less frequently tubular piezoelectric transducers (Marszal *et al.*, 2005). With this configuration of hydrophones in the system, it is only possible to determine the bearing of the signal source, which is still sufficient for most applications. The signals from hydrophone pairs (H1, H3, and H2, H4) are subtracted, filtered by the low-pass filter (LPF), and the difference between them is subjected to Fast Fourier Transform (FFT). Fourier transform is also determined for the signal received by the central hydrophone H0.

An alternative system configuration is possible, in which the central hydrophone is not used, as shown in Fig. 2.

Assuming initially that only useful signal $s(t)$ without noise is received and that the signal source is at a long distance R from the antenna and that $R \gg 2d$,

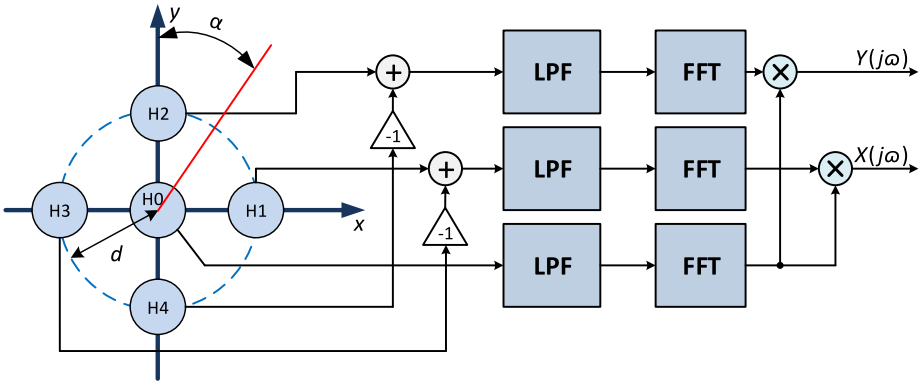

Fig. 1. Functional diagram of a DIFAR system.

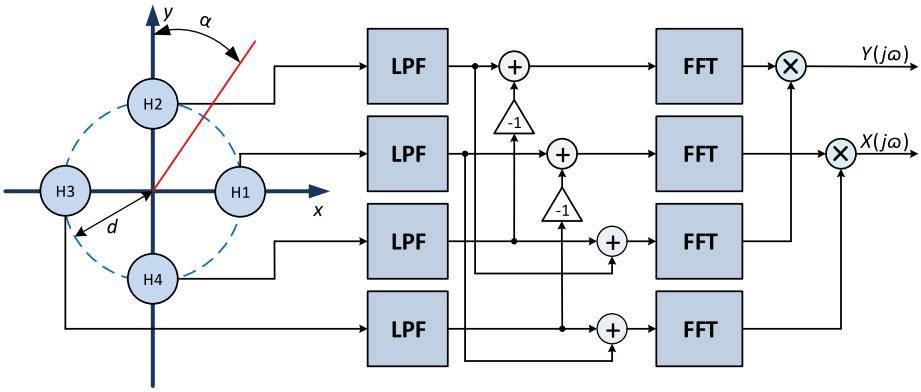

Fig. 2. Functional diagram of an alternative system with four hydrophones.

the method of processing in the system configured as shown in Fig. 1 is described by the following dependencies:

$$\begin{aligned}\Im\{s_1(t)-s_3(t)\} &= \Im\{s(t+\tau_s)-s(t-\tau_s)\}\\ &= (e^{j\omega\tau_s}-e^{-j\omega\tau_s})S(j\omega)\\ &= 2j\sin\omega\tau_s\cdot S(j\omega), \qquad (1)\end{aligned}$$

$$\begin{aligned}\Im\{s_2(t)-s_4(t)\} &= \Im\{s(t+\tau_c)-s(t-\tau_c)\}\\ &= (e^{j\omega\tau_c}-e^{-j\omega\tau_c})S(j\omega)\\ &= 2j\sin\omega\tau_c\cdot S(j\omega), \qquad (2)\end{aligned}$$

where $s_1(t),...,s_4(t)$ are the signals received by individual hydrophones, $2d$ is the delays depend on the hydrophones' distance, c is speed of the acoustic wave in water, and α is bearing, equal to $\tau_s = \frac{d}{c}\sin\alpha$ and $\tau_c = \frac{d}{c}\cos\alpha$. The Fourier transform of the signal $s(t)$ is determined as: $\Im\{s(t)\} = S(j\omega)$.

The multiplication of the above expressions by $S^*(j\omega)$ results in the following:

$$\begin{aligned}X(j\omega) &= 2j\sin\omega\tau_s\cdot|S(j\omega)|^2\\ &\cong 2j\omega\frac{d}{c}\sin\alpha\cdot|S(j\omega)|^2, \qquad (3)\end{aligned}$$

$$\begin{aligned}Y(j\omega) &= 2j\sin\omega\tau_c\cdot|S(j\omega)|^2\\ &\cong 2j\omega\frac{d}{c}\cos\alpha\cdot|S(j\omega)|^2, \qquad (4)\end{aligned}$$

because the argument of the sine function is very small – close to zero.

The above equations may be used to determine bearing α, which is the same at each frequency of the received signal spectrum. Bearing α is described as:

$$\alpha = \operatorname{arctg}\frac{X(j\omega)}{Y(j\omega)}. \qquad (5)$$

In the alternative version of the system shown in Fig. 2, the sums of the received signals are used, which results in the following:

$$\begin{aligned}\Im\{s_1(t)+s_3(t)\} &= \Im\{s(t+\tau_s)+s(t-\tau_s)\}\\ &= (e^{j\omega\tau_s}+e^{-j\omega\tau_s})S(j\omega)\\ &= 2\cos\omega\tau_s\cdot S(j\omega), \qquad (6)\end{aligned}$$

$$\begin{aligned}\Im\{s_2(t)+s_4(t)\} &= \Im\{s(t+\tau_c)+s(t-\tau_c)\}\\ &= (e^{j\omega\tau_c}+e^{-j\omega\tau_c})S(j\omega)\\ &= 2\cos\omega\tau_c\cdot S(j\omega). \qquad (7)\end{aligned}$$

The multiplication of the expressions described by formulae (1) and (2) by the coupled spectra given by the above formulae results in the following:

$$\begin{aligned}X(j\omega) &= 4j\sin\omega\tau_s\cos\omega\tau_s\cdot|S(j\omega)|^2\\ &= 2j\sin 2\omega\tau_s\cdot|S(j\omega)|^2, \qquad (8)\end{aligned}$$

$$\begin{aligned}Y(j\omega) &= 4j\sin\omega\tau_c\cos\omega\tau_c\cdot|S(j\omega)|^2\\ &= 2j\sin 2\omega\tau_c\cdot|S(j\omega)|^2. \qquad (9)\end{aligned}$$

In the antenna without of central hydrophone H0, as in the previous case, results in the following:

$$\begin{aligned}X(j\omega) &= 2j\sin 2\omega\tau_s\cdot|S(j\omega)|^2\\ &\cong 4j\omega\frac{d}{c}\sin\alpha\cdot|S(j\omega)|^2, \qquad (10)\end{aligned}$$

$$\begin{aligned}Y(j\omega) &= 2j\sin 2\omega\tau_c\cdot|S(j\omega)|^2\\ &\cong 4j\omega\frac{d}{c}\cos\alpha\cdot|S(j\omega)|^2, \qquad (11)\end{aligned}$$

because for the very small argument of the cosine function it has a value close to one.

The advantage of this method is the possibility of simplifying the system antenna design, however the number of received signal processing operations is increased.

In both versions of the system, errors of bearing α depend on the input signal-to-noise ratio SNR. This will be determined further in this paper by simulating the numerical operation of the system. For this purpose, the following algorithms will be used:

- for the system with a central hydrophone:

$$\begin{aligned}X(j\omega) = \operatorname{Im}[&\Im\{s(t+\tau_s)-s(t-\tau_s)+n_1(t)-n_3(t)\}\\ &\cdot\Im^*\{s(t)+n(t)\}], \qquad (12)\end{aligned}$$

$$\begin{aligned}Y(j\omega) = \operatorname{Im}[&\Im\{s(t+\tau_c)-s(t-\tau_c)+n_2(t)-n_4(t)\}\\ &\cdot\Im^*\{s(t)+n(t)\}], \qquad (13)\end{aligned}$$

- for the system without a central hydrophone:

$$\begin{aligned}X(j\omega) = \operatorname{Im}[&\Im\{s(t+\tau_s)-s(t-\tau_s)+n_1(t)-n_3(t)\}\\ &\cdot\Im^*\{s(t+\tau_s)+s(t-\tau_s)+n_1(t)+n_3(t)\}], \qquad (14)\end{aligned}$$

$$\begin{aligned}Y(j\omega) = \operatorname{Im}[&\Im\{s(t+\tau_c)-s(t-\tau_c)+n_2(t)-n_4(t)\}\\ &\cdot\Im^*\{s(t+\tau_c)+s(t-\tau_c)+n_2(t)+n_4(t)\}], \qquad (15)\end{aligned}$$

where $n(t),...,n_4(t)$ represent the noise received by hydrophones with specific numbers.

The algorithms written above are processed in the numerical system. In addition, the signal received is filtered by analogue low-pass filters to reduce the noise band and meet regular sampling requirements, although this is not included in the above formulae.

3. Numerical model of the system

The numerical processing of the operations described above required the development of a model of

noise that will be acceptably close to the real ambient noise field. However, the reflection of the wave from the bottom and the sea surface was omitted and a constant spatial distribution of the speed of sound was assumed. For this purpose, the system antenna was surrounded with a very large number of noise sources with a random and homogeneous spatial distribution in a sphere with a selectable radius. Each source emitted an independent execution of Gaussian noise, with an identical duration and identical variance. An example distribution of noise sources is shown in Fig. 3.

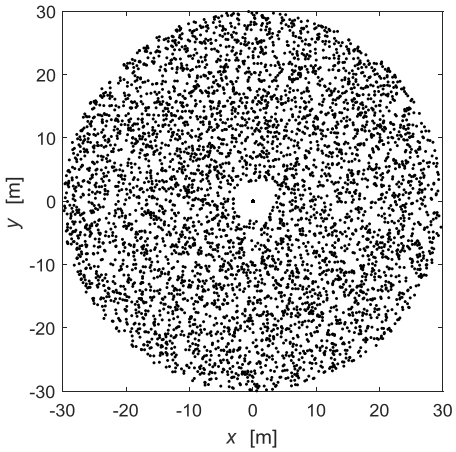

Fig. 3. Cross-section of surface distribution of noise sources.

Due to the symmetry of the model, the research can be limited to one pair of hydrophones. Assuming a Cartesian coordinate system, it is assumed that the coordinates of a pair of hydrophones are as follows: $x_1 = -d$, $y_1 = 0$, $z_1 = 0$, and $x_3 = d$, $y_3 = 0$, $z_3 = 0$. If the coordinates of a certain noise source are x, y, z, then its distances from the hydrophones are as follows:

$$\begin{aligned} R &= \sqrt{x^2 + y^2 + z^2}, \\ R_1 &= \sqrt{(x+d)^2 + y^2 + z^2}, \\ R_3 &= \sqrt{(x-d)^2 + y^2 + z^2}, \end{aligned} \tag{16}$$

where R represents the distance to the central hydrophone, R_i – distance to the i-th hydrophone.

Assuming a spherical model of propagation, the noise received by the hydrophones can be expressed as follows:

$$\begin{aligned} n(t) &= \frac{\sigma R_0}{R} f[t - \tau(R)], \\ n_1(t) &= \frac{\sigma R_0}{R_1} f[t - \tau_1(R_1)], \\ n_3(t) &= \frac{\sigma R_0}{R_3} f[t - \tau_3(R_3)], \end{aligned} \tag{17}$$

where R_0 is the reference distance (e.g. $R_0 = 1$ m), the delays are as follows: $\tau = R/c$, $\tau_1 = R_1/c$, $\tau_3 = R_3/c$, while c represents the speed of the acoustic wave in water.

In numerical calculations, continuous time t must be converted to discrete time-series separated by the sampling time Δt, i.e. $t = k\Delta t = k/f_s$, where f_s is the sampling frequency. The sampling frequency should be selected to reflect the actual delays τ with sufficient accuracy. In the considered system, the difference of delays between hydrophones 1 and 3 is essential, i.e. $\Delta t_{13} = \tau_1(R_1) - \tau_3(R_3)$. The determination of $2a = c\Delta t_{13}$ and the use of formula (16) result in the following:

$$\sqrt{(x+d)^2 + y^2 + z^2} - \sqrt{(x-d)^2 + y^2 + z^2} = 2a. \tag{18}$$

After transforming the above formula, it is found that coordinates x, y, z of the noise source meet the following equation:

$$\frac{x^2}{a^2} - \frac{y^2}{b^2} - \frac{z^2}{b^2} = 1, \tag{19}$$

where $d^2 = a^2 + b^2$.

This is the equation of a rotary hyperboloid with foci $(-d, 0, 0)$ and $(d, 0, 0)$, of which the traces on surface $z = 0$ are shown in Fig. 4. This was noticed i.e. by (Roux *et al.*, 2005).

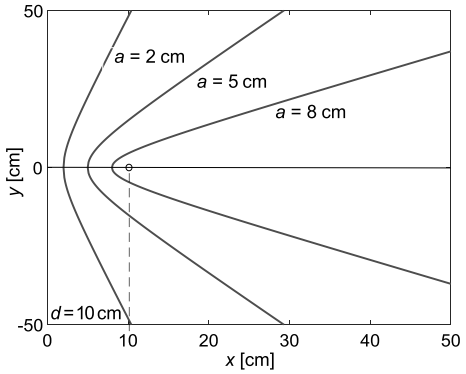

Fig. 4. Traces of right rotary hyperboloids.

In numerical calculations, it should be assumed that delay Δt_{13} is an integer multiple p of the sampling time Δt, i.e. $\Delta t_{13} = p\Delta t = p/f_s$. Consequently, for a hydrophone distance of $2d$, $2d = cP/f_s$ should be equally true, where P is a natural number. The number P is equal to the number of hyperboloid branches, on which noise sources have delay difference Δt_{13}. It determines the accuracy of delay measurements and thus influences the quality of the model of noise. With the assumed hydrophone distance $2d$ and the assumed number P, the sampling frequency is as follows:

$$f_s = \frac{cP}{2d}. \tag{20}$$

It should be noted, that the discretisation of time is inconsistent with the assumption of uniform spatial distribution of the noise sources. The individual sources are subject to an apparent shift towards the

nearest hyperboloid. However, their position on the appropriate hyperboloid remains random. Further in this paper, it will be investigated whether this has an impact on the quality of the model. This quality is evaluated by analysing the values of the Pearson correlation coefficient r_{p13}, the correlation function $r_{13}(t)$, and the difference of spectra of the noise received by the hydrophones.

The numerical procedure for determining the correlation function is completed in the following steps:

- determination of the spatial uniform distribution N of the noise sources,
- calculation from formulae (16) of distances $R(n)$, $R_1(n)$, and $R_3(n)$ of every n source,
- determination of the number of delay samples: $p(n) = \text{int}[R(n) \cdot f_s/c]$, $p_1(n) = \text{int}[R_1(n) \cdot f_s/c]$, $p_3(n) = \text{int}[R_3(n) \cdot f_s/c]$,
- generation of K Gaussian noise samples $n(k)$ (where k is sequential number of noise sample) with a standard deviation σ – further also referred to as std(·), and filtering them by the Butterworth filter with degree 8 and spectrum width B,
- delaying the set of consecutive samples by predetermined delays,
- calculation of the sum of samples according to formulae:

$$\begin{aligned} s(k) &= \sum_{n=1}^{n=N} \frac{\sigma R_0}{R(n)} n\,[k - p(n)], \\ s_1(k) &= \sum_{n=1}^{n=N} \frac{\sigma R_0}{R_1(n)} n\,[k - p_1(n)], \\ s_3(k) &= \sum_{n=1}^{n=N} \frac{\sigma R_0}{R_3(n)} n\,[k - p_3(n)], \end{aligned} \tag{21}$$

- calculation of discrete Fourier transforms:

$$\begin{aligned} S(k) = \Im\{s(n)\}, \qquad S_1(k) = \Im\{s_1(n)\}, \\ \text{and} \quad S_3(k) = \Im\{s_3(n)\}, \end{aligned} \tag{22}$$

- determination of the correlation function using the fast Fourier transform method, according to the formula:

$$\gamma_{1-3}(k) = \Im^{-1}\{\Im[S_1(k)] \cdot \Im[S_3(k)]\}. \tag{23}$$

The differences of spectra $S_1(k) - S_3(k)$ are calculated using formulae (22). In the following figures, typical correlation functions and spectra differences are shown, normalised for maximum values. They are averaged over five measurement cycles with duration T. They are subject to certain changes depending on the assumed parameters, which will be shown further on. In Fig. 7, the frequency range around zero should be noted, in which very small values are assumed. It is useful from the point of view of the considered system.

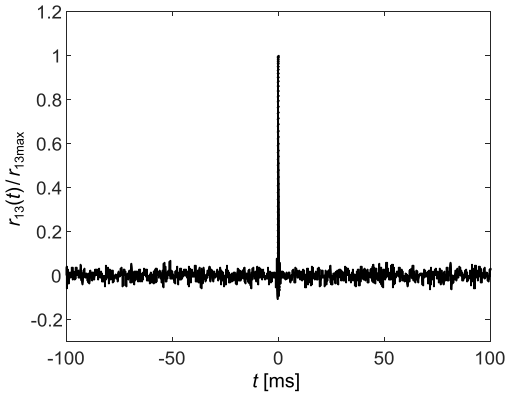

Fig. 5. Noise correlation function ($2d$ = 0.2 m, N = 8000, f_s = 150 kHz, B = 2 kHz, T = 0.2 s, σ = 0.81, r_{p13} = 0.77).

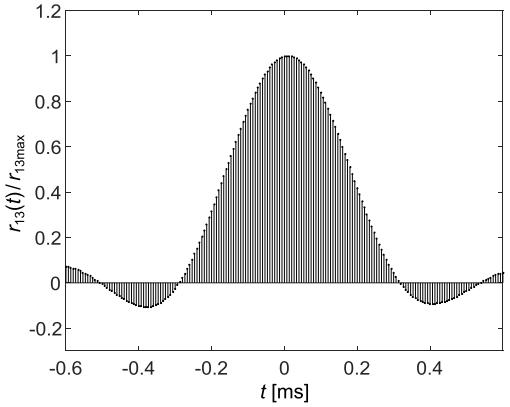

Fig. 6. Central section of the correlation function from Fig. 5.

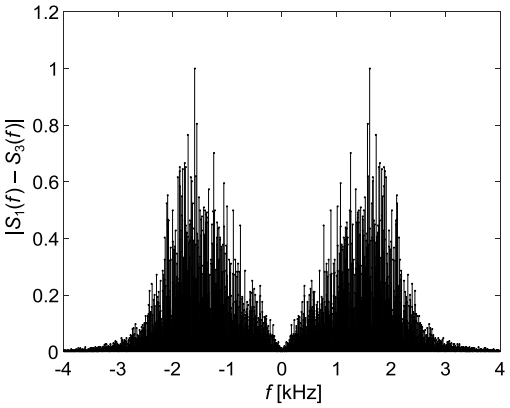

Fig. 7. The spectra difference of noise received by hydrophones 1 and 3 (parameters as in Fig. 5).

The above-discussed limitations of the digital simulation of the system are not applicable to the received sinusoidal signals, in which delays can be replaced with a phase shift. For example, for a sinusoidal signal with frequency f_0, the formula (1) in discrete notation is as follows:

$$\begin{aligned} \Im\{s_1(k) - s_3(k)\} &= \Im\left\{\sin\left(2\pi k \frac{f_0}{f_s} + \varphi_s\right) - \sin\left(2\pi k \frac{f_0}{f_s} - \varphi_s\right)\right\} \\ &= (e^{j\varphi_s} - e^{-j\varphi_s}) S(k) = 2j \sin\varphi_s \cdot S(k). \end{aligned} \tag{24}$$

As shown – regardless of the sampling frequency f_s – for a sinusoidal signals, spectral lines amplitudes are proportional to sines of phase shifts $\varphi_s = 2\pi f_0 \tau_s$.

To select the parameters of the numerical model of noise, first the impact of the sampling frequency f_s will be examined, while maintaining constant values of the other parameters. The example averaged result of calculations is shown in Table 1. As shown and confirmed by other calculations, the values of correlation coefficients are practically identical and independent of the sampling frequency. Moreover, this frequency has no impact on the course of the correlation function and spectra difference. The basic criterion of numerical correctness of the model of the noise is thus met.

Table 1. Coefficient dependency.

f_s [kHz]	r_{p13}	r_{p24}
75	0.778	0.770
150	0.786	0.778
225	0.789	0.786
300	0.785	0.770
$2d$ = 0.2 m, N = 8000, B = 2 kHz, T = 0.2 s		

Table 2 illustrates the impact of the number of sources on the correlation coefficient value. The number of sources was changed with a constant observation range R, while changing the bulk density. The results included show that at the number of sources of approx. 1000, the correlation coefficients are practically constant, which means that this number of sources is sufficient for use in the model.

Table 2. Impact of N noise sources on sampling frequency correlation coefficients.

N	r_{p13}	std(r_{p13})	r_{p24}	std(r_{p24})
4000	0.776	0.020	0.789	0.021
8000	0.781	0.014	0.772	0.017
1200	0.784	0.018	0.772	0.020
1600	0.782	0.014	0.771	0.018
$2d$ = 0.2 m, R = 40 m, f_s = 150 kHz, B = 2 kHz, T = 0.2 s				

Moreover, it was checked, whether the model of noise retained its properties with a changed observation range R and fixed number of sources. Example results are shown in Table 3.

Table 3. Dependency of the correlation coefficients on the range of observation R.

R [m]	r_{p13}	std(r_{p13})	r_{p24}	std(r_{p24})
30	0.790	0.015	0.778	0.014
40	0.781	0.019	0.781	0.010
50	0.772	0.010	0.780	0.017
60	0.771	0.026	0.773	0.028
$2d$ = 0.2 m, N = 10000, f_s = 150 kHz, B = 2 kHz, T = 0.2 s				

In the observation range given in the table, correlation coefficient values show no significant changes. The increase of the standard deviation was only noted at longer ranges, which is related to the fast decrease of the bulk density of the sources.

In conclusion, the calculations proved the correct functioning of the numerical model of noise across a relatively wide range of parameters. In the further analyses, the model will be used with fixed parameters, namely: sampling frequency f_s = 150 kHz, number of sources N = 10000 and observation range R = 50 m. The sources around the antenna, within a sphere with a radius of 3 m, will be eliminated. Statistically, this area includes 2 sources, but the noise they emit can have a very high standard deviation, which is also different for each hydrophone. This disturbs the statistical image of the calculation results.

Table 4 and the figures below illustrate the impact of hydrophone distance $2d$ on the correlation coefficient values, the duration of the correlation function t_c and its courses. The duration of the correlation function was determined as the time range between the first zeroes of this function.

Table 4. The dependency of the correlation coefficients and the duration of the correlation on hydrophone distance $2d$.

$2d$ [m]	r_{p13}	r_{p24}	t_c [ms]
0.1	0.940	0.938	0.54
0.2	0.778	0.787	0.6
0.4	0.561	0.551	0.94
0.6	0.318	0.317	1.2
0.8	0.167	0.124	1.5
1.0	0.128	0.158	1.7
R = 50 m, N = 10000, f_s = 150 kHz, B = 2 kHz, T = 0.2 s			

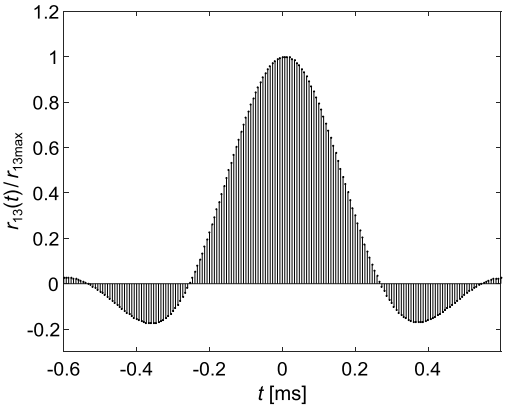

Fig. 8. Correlation function with hydrophone distance $2d$ = 0.1 m.

As the hydrophones' distance increased, the correlation coefficient values decrease quickly and the duration of the correlation function increases. This means that the correlation between the noise received

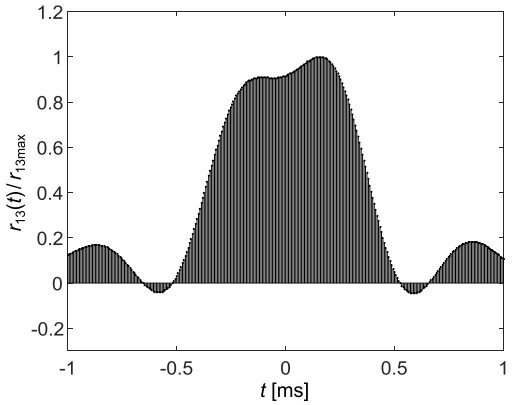

Fig. 9. Correlation function with hydrophone distance $2d = 0.4$ m.

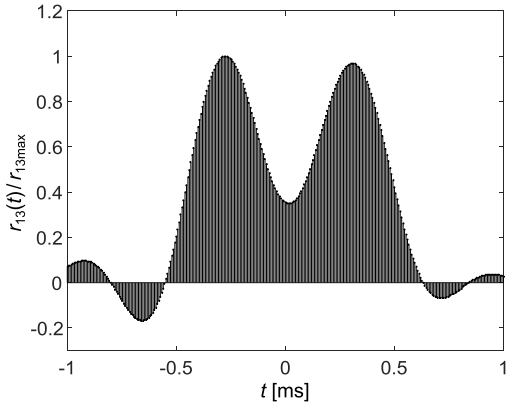

Fig. 10. Correlation function with hydrophone distance $2d = 0.6$ m.

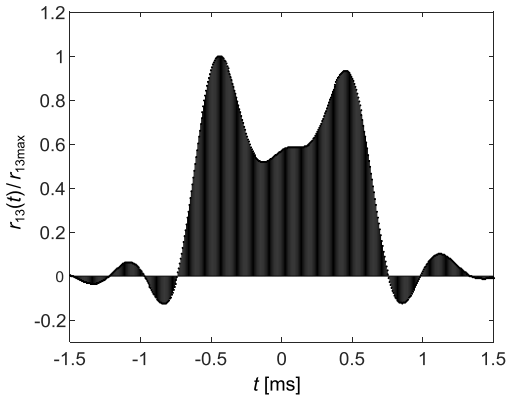

Fig. 11. Correlation function with hydrophone distance $2d = 0.8$ m.

by the hydrophones deteriorates. In general, the duration of the correlation function depends on the doubled time of the acoustic wave propagation between the hydrophones. For example, for a distance of $2d = 0.6$ m, this time is 0.8 s, which is smaller than time $t_c = 1.2$ s. This regularity is applicable to all hydrophone distances given in Table 4. As shown below, this is related to the noise spectrum width.

Table 5 includes the correlation coefficient values and the effective length of the correlation function for

Table 5. The dependency of the correlation coefficients and the duration of the correlation on noise spectrum width.

B [kHz]	r_{p13}	r_{p24}	t_c [ms]
1	0.939	0.943	1.0
4	0.561	0.554	0.56
10	0.130	0.133	0.34
30	0.042	0.037	0.28
$2d = 0.2$ m, $R = 50$ m, $N = 10000$, $f_s = 150$ kHz, $T = 0.2$ s			

varied noise bandwidths B, while the figures below show typical correlation function courses. The figures were prepared with the parameters given in Table 5.

An increase in the noise spectrum width results in a deteriorated correlation, which is shown by the quickly decreasing correlation coefficient values. At the same time, the duration of the correlation function approaches the doubled time of the wave propagation between the hydrophones. This time is $4d/c = 0.4$ m$/1500$ ms $= 0.27$ ms. As the spectrum width increases, the noise properties approach the Dirac distribution properties, while the correlation function for the signal includes two pulses with a time span of 0.27 ms. Approaching this situation is shown in Figs 13 and 14.

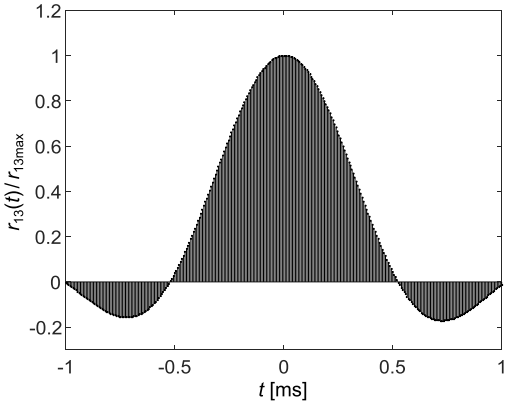

Fig. 12. Noise correlation function with spectrum width $B = 1$ kHz.

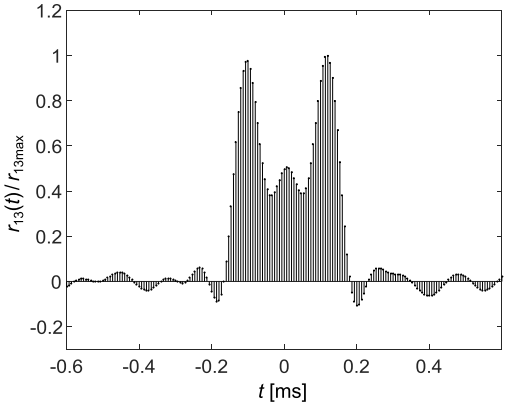

Fig. 13. Noise correlation function with spectrum width $B = 10$ kHz.

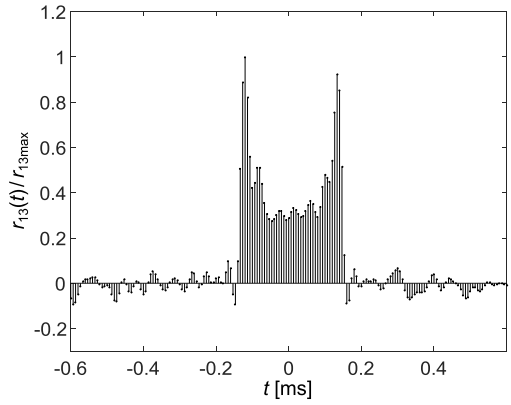

Fig. 14. Noise correlation function with spectrum width B = 30 kHz.

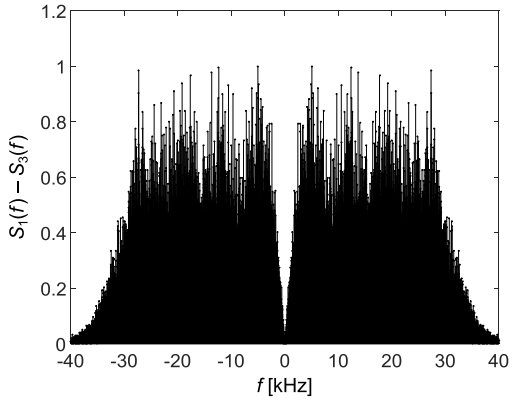

Fig. 15. Difference of noise spectra from Fig. 14.

The increase of the noise spectrum width is accompanied by an increase in variance, i.e. deterioration of the signal-to-noise ratio. This has an adverse impact on bearing errors, which will be shown in the next section.

The impact of the spectrum width on the correlation function shown here has little relevance to practical systems, in which the spectrum width of received noise does not exceed single digit kHz (Salamon, 2004; 2006; Marszal *et al.*, 2005). This is only to confirm, from a physical point of view, the correct operation of the presented numerical model of centre noise.

In general, the above correlation functions using the numerical model of noise meet the theoretical results obtained by theoretical and experimental means, included for example in publications: (Barclay, Buckingham, 2016) – Figs 7 and 8, (Barclay, Buckingham, 2014) – Figs 13 and 14, and (Buckingham 2012) – Fig. 11. A more complete conformity can be expected after supplementing the presented model of noise with a numerical model of wave noise, which will be the subject of the next publication.

4. Simulation research on the system

The numerical model of the acoustic noise of the sea presented above was used to examine its impact on the operation of two versions of the system described in Sec. 2. The objective of this examination was to determine the impact of noise correlation on bearing errors as a function of:

- input signal-to-noise ratio SNR,
- hydrophone distance $2d$,
- received signal frequency f_0,
- noise spectrum width B,
- the type of the received signal.

At the same time, the equivalence of both versions of the system will be verified. For this purpose, the bearing obtained in the system without a central hydrophone is marked with a circle, and the bearing from the system with a central hydrophone is marked with an asterisk. To show the impact of noise correlation on bearing accuracy, the bearing obtained for non-correlated noise will be given for comparison.

The impact of noise on bearing accuracy is illustrated by Table 6 and Figs 16 and 17. The figures show the results of 10 tests. Calculations were made based on the numerical model of noise described above. Subsequent values of signal-to-noise ratio SNR were assumed with the variance σ^2 and standard deviation σ calculated on the output of the selected hydrophone after low-pass filtering, then amplitude s_0 was determined for the sine signal with frequency f_0, using the formula:

$$s_0 = \sqrt{2}\sigma 10^{\mathrm{SNR}/20}. \tag{25}$$

Based on the results in the table and on the graphical presentation of bearing values, it was concluded that systems with and without a central hydrophone are fully equivalent. Beyond SNR = –5 dB, bearing accuracy improves visibly. With a worse signal-to-noise ratio, high errors occur, which makes the system useless in practice.

Table 6. Impact of signal-to-noise ratio SNR on bearing errors.

	SNR [dB]	–5	0	5	10	15
Without central hydrophone	$\overline{\Delta\alpha}$ [deg]	1.02	0.65	–0.21	–0.06	–0.05
	std($\Delta\alpha$) [deg]	2.20	1.31	0.46	0.28	0.20
With central hydrophone	$\overline{\Delta\alpha}$ [deg]	1.04	0.66	–0.20	–0.05	–0.04
	std($\Delta\alpha$) [deg]	2.20	1.31	0.46	0.28	0.20
f_0 = 100 Hz, f_s = 150 kHz, B = 2 kHz, T = 0.2 s, $2d$ = 0.2 m, N = 10000, r_{p13} = 0.79						

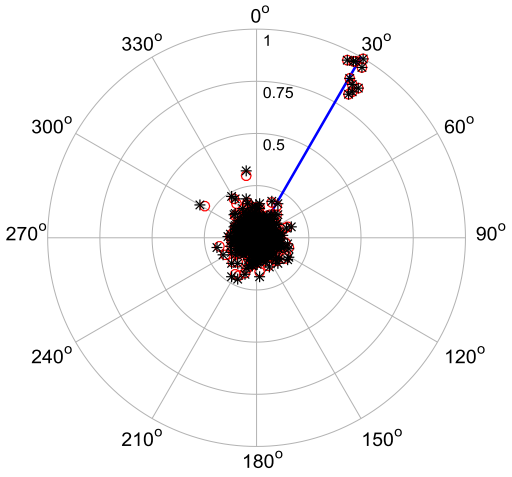

Fig. 16. Signal source bearing $\alpha = 30°$, SNR = −5 dB ($2d$ = 0.2 m, R = 50 m, N = 10000, f_s = 150 kHz, f_0 = 100 Hz, T = 0.2 s).

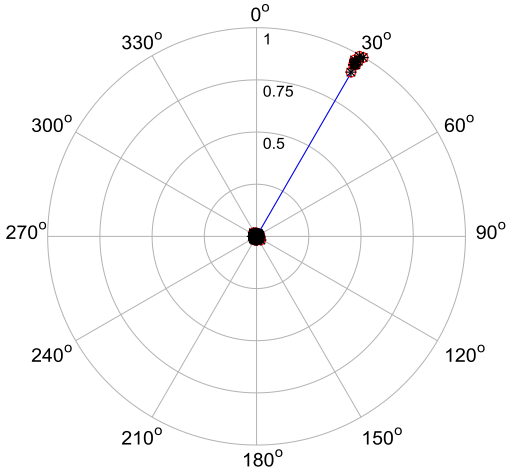

Fig. 17. Signal source bearing $\alpha = 30°$, SNR = 5 dB (other parameters as in Fig. 16).

Table 7 includes the results of bearing calculations as a function of hydrophone distance, while maintaining constant values of the other parameters. The results are averaged over ten simulations.

Despite the deterioration of the noise correlation as the hydrophone distance increased, both the average bearing error and its standard deviation show no distinctive trends. Their dispersions are within statistical error with a relatively small number of tests. Thus it can be concluded that bearing accuracy does not depend on the hydrophone distance across a wide range of variation. It results from the fact that the deteriorating noise correlation (drop of the correlation coefficient) is compensated by the increasing difference between the sine signals received by the hydrophones.

Bearing accuracy is also influenced by the received signal frequency, as shown in Table 8 and illustrated by the example bearing values shown in Fig. 18. The reason is the differences between the received noise spectra shown in Fig. 19. The compensating impact of the sine signal difference value increasing with frequency is however only efficient in the example shown starting from frequencies higher than 20 Hz. However, this limit is not constant and depends on the signal-to-noise ratio and distance between hydrophones.

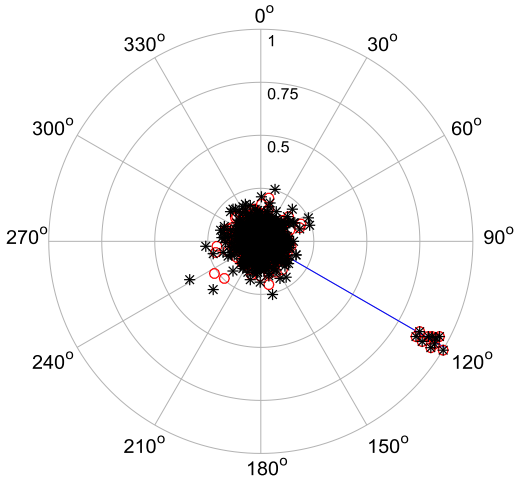

Fig. 18. Example bearing at frequency f_0 = 20 Hz ($2d$ = 0.4 m, f_s = 150 kHz, B = 2 kHz, T = 0.2 s, SNR = 0 dB, N = 10000, $\alpha = 120°$).

Table 7. Impact of hydrophone distance $2d$ on bearing errors.

$2d$ [m]	0.1	0.2	0.4	0.6	0.8	1.0
$r_{p_{13}}$	0.96	0.80	0.56	0.35	0.19	0.17
$\overline{\Delta\alpha}$ [deg]	−0.44	0.09	0.13	0.15	−0.32	−0.18
std($\Delta\alpha$) [deg]	1.72	0.96	1.45	1.15	1.00	1.59
f_0 = 100 Hz, f_s = 150 kHz, B = 2 kHz, T = 0.2 s, SNR = 0 dB, N = 10000, $\alpha = 45°$						

Table 8. The dependency of bearing on the received signal frequency.

f_0 [Hz]	10	20	50	100	200
$\overline{\Delta\alpha}$ [deg]	−2.12	0.17	−0.19	0.38	−0.56
std($\Delta\alpha$) [deg]	3.57	1.37	1.96	1.22	1.07
$2d$ = 0.4 m, f_s = 150 kHz, B = 2 kHz, T = 0.2 s, SNR = 0 dB, N = 10000, $\alpha = 120°$					

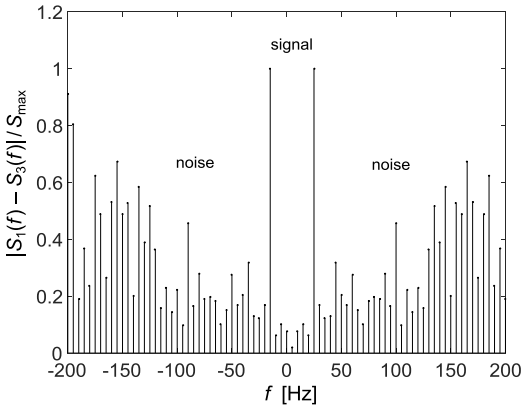

Fig. 19. Spectra difference of signal with noise received by hydrophones (parameters as in Fig. 18).

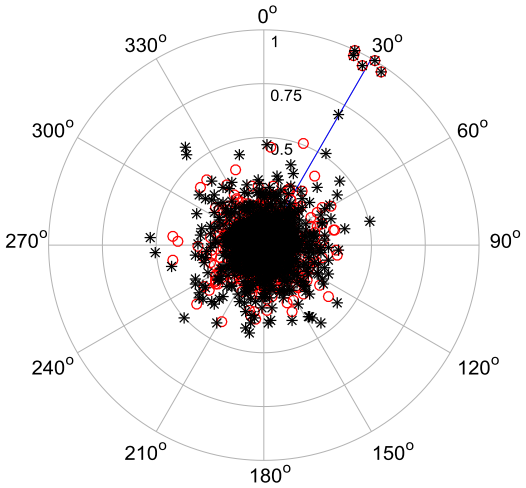

Fig. 20. Bearing with spectrum width B = 4 kHz (f_0 = 100 Hz, $2d$ = 0.2 m, f_s = 150 kHz, T = 0.2 s, SNR = −7 dB, N = 10000, α = 30°).

The noise spectrum width resulting from filtering by the low-pass filter has a direct impact on the noise level and thus on the signal-to-noise ratio. The dependency of the signal-to-noise ratio in the numerical calculations is described by the following formula:

$$\mathrm{SNR} = 10\log\frac{s_0^2}{2\sigma^2} + 10\log\frac{f_s}{B}, \tag{26}$$

where the first component describes the signal-to-noise ratio without filtering, and the second component expresses the increase of the ratio caused by filtering. The impact of the signal-to-noise ratio on bearing errors is shown in Table 6.

The noise spectrum width also influences the noise correlation level, which is illustrated by Table 5 and Figs 15–18. The question is whether the noise correlation has an impact on bearing errors. This is answered by the results of the calculations shown in Table 9.

With the signal-to-noise ratio in the range given in the table, the noise spectrum width shows no visible distinctive trends. The dispersion of values results from statistical errors. The same effect is visible in Table 6. At lower SNR values, the error also does not increase with increasing spectral width. On the other hand, the background noise in the center of the plot increases as shown in Fig. 20, which may result in incorrect detection of maximum spectral lines. The system provides worse measurement accuracy when the received signal is a periodical rectangular wave ($\overline{\Delta\alpha}$ = −1.29°, std($\Delta\alpha$) = 2.09°, for sine signal $\overline{\Delta\alpha}$ = −0.21°, std($\Delta\alpha$) = 0.46°). Example bearings are shown in Fig. 21. Delay rounding, which is necessary in the simulations, caused a bearing error of $\overline{\Delta\alpha}$ = −2.1°. This error is not constant, but depends on the delay rounding for the given bearing. It is caused by the apparent shift of noise sources to the surface of the rotary

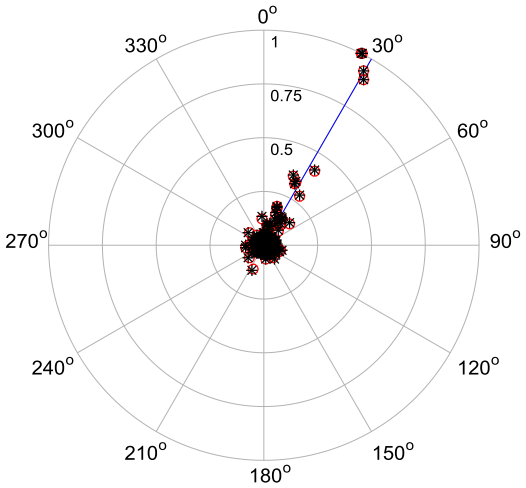

Fig. 21. Rectangular wave bearing (f_0 = 100 Hz, $2d$ = 0.2 m, f_s = 150 kHz, T = 0.2 s, SNR = 5 dB, N = 10000, α = 30°).

Table 9. Impact of the bandwidth on bearing errors.

B [kHz]	1	2	3	4	5
SNR [dB]	5.1	2.0	0.2	−1.1	−2.1
r_{p13}	0.96	0.81	0.71	0.55	0.39
$\overline{\Delta\alpha}$ [deg]	0.19	0.02	−0.05	0.31	0.17
std($\Delta\alpha$) [deg]	0.61	0.86	1.04	1.32	0.97
$2d$ = 0.2 m, s_0 = 1, σ = 1, f_0 = 100 Hz, f_s = 150 kHz, T = 0.2 s, N = 10000, α = 30°					

Table 10. Impact of the signal-to-non-correlated noise ratio on bearing errors.

SNR [dB]	10	15	20	25	30
$\overline{\Delta\alpha}$ [deg]	0.12	−0.18	2.09	−0.12	−0.51
std($\Delta\alpha$) [deg]	7.8	4.3	2.4	1.6	0.5
$2d$ = 0.2 m, f_0 = 50 Hz, f_s = 150 kHz, B = 2 kHz, T = 0.2 s, N = 10000, α = 30°					

hyperboloids, which is discussed in Sec. 3. It should be emphasised that this is a simulation error, and is not present in the actual system.

Along the bearing line, bearing values appear as determined for the subsequent band of the rectangular wave spectrum.

In the end, it will be shown how noise correlation reduces bearing errors compared to a situation in which the hydrophones receive non-correlated Gaussian noise. In each cycle with duration T, the hydrophones independently receive ten N noise executions with spectrum width B, while the results are averaged over ten measurement cycles. Table 10 includes bearing errors as a function of signal-to-noise ratio SNR.

For SNR values smaller than 10 dB, the bearing values show no distinctive concentration and thus they are not included in the table. Comparing the results in the above table with the results given in Table 6, similar bearing errors occur for the non-correlated noise, when the signal-to-noise ratio is approx. 25 dB greater than for the correlated noise. As shown in Fig. 22, large bearing errors occur despite the high signal-to-noise ratio, which manifests itself by a very high concentration of false resolutions in the central section of the plot. Figure 23 shows spectra differences, which do not accept small values, typical of correlated noise, shown in Figs 7 and 15, in the low frequency range. This explains the significantly worse system properties when receiving non-correlated signals.

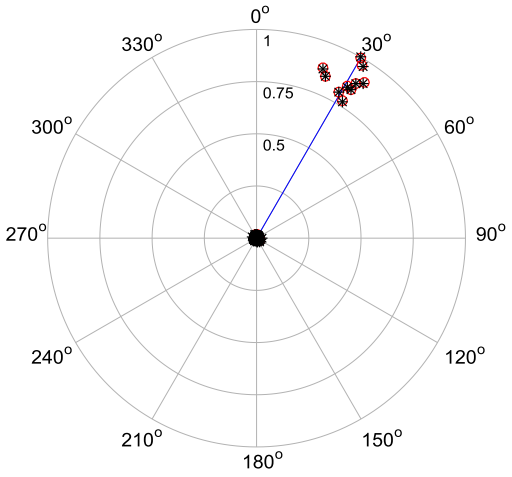

Fig. 22. Example bearing for non-correlated noise ($2d$ = 0.2 m, f_s = 150 kHz, B = 2 kHz, T = 0.1 s, SNR = 15 dB, N = 10000, α = 30°, r_{p13} = 0.023.

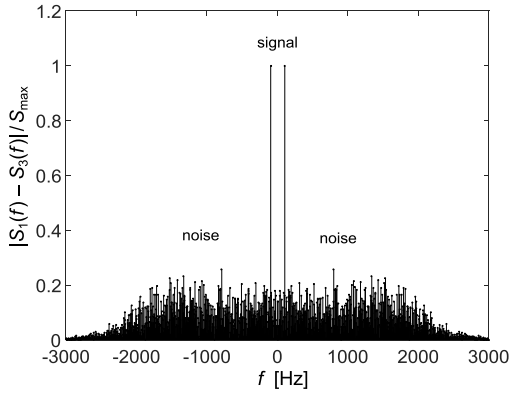

Fig. 23. Spectra difference of signal with noise received by hydrophones (parameters as in Fig. 22).

5. Conclusions

The calculations provided in Sec. 3 have proven that the proposed numerical model of sea noise simulates the reception of noise in the considered system in a satisfactory manner. This requires, however, supplementing by a numerical model of wind-driven sea waves noise, bringing it closer in order to better simulate/reproduce the real conditions in the sea. Application of the developed model of noise enabled comprehensive testing of the impact of the main system parameters on bearing accuracy.

A system with a central hydrophone was considered to be equivalent to a system without a hydrophone, which increases design flexibility.

It was shown that adopting the non-correlated noise model in the simulation system leads to false results, which are unacceptable in practice.

References

1. Barclay D.R., Buckingham M.J. (2014), On the spatial properties of ambient noise in the Tonga Trench, including effects of bathymetric shadowing, *The Journal of the Acoustical Society of America*, **136**(5): 2497–2511, doi: 10.1121/1.4896742.

2. Barclay D.R., Buckingham M.J. (2016), Depth dependence of wind-driven, broadband ambient noise in the Philippine Sea, *The Journal of the Acoustical Society of America*, **133**(1): 62–71, doi: 10.1121/1.4768885.

3. Buckingham M.J. (2012), Cross-correlation in band-limited ocean ambient noise fields, *The Journal of the*

Acoustical Society of America, **131**(4): 2643–2657, doi: 10.1121/1.3688506.

4. Buckingham M.J. (2011), On the two-point cross-correlation function of anisotropic, spatially homogeneous ambient noise in the ocean and its relationship to the Green's function, *The Journal of the Acoustical Society of America*, **129**(6): 3562–3576, doi: 10.1121/1.3573989.
5. Burdick W.S. (1984), *Underwater Acoustic System Analysis*, Prentice-Hall, Englewood Cliffs, NJ.
6. Cox H. (1973), Spatial correlation in arbitrary noise fields with application to ambient sea noise, *The Journal of the Acoustical Society of America*, **54**(5): 1289–1301, doi: 10.1121/1.1914426.
7. Cron B.F., Sherman C.H. (1962), Spatial-correlation functions for various noise models, *The Journal of the Acoustical Society of America*, **34**(11): 1732–1736, doi: 10.1121/1.1909110.
8. Greene Jr. C.R., McLennan M.W., Norman R.G. (2004), Directional frequency and recording (DIFAR) sensors in seafloor recorders to locate calling bowhead whales during their fall migration, *The Journal of the Acoustical Society of America*, **116**(2): 799–813, doi: 10.1121/1.1765191.
9. Grelowska G., Kozaczka E., Kozaczka S., Szymczak W. (2013), Underwater noise generated by small ships in the shallow sea, *Archives of Acoustics*, **38**(3): 351–356. doi: 10.2478/aoa-2013-0041.
10. Klusek Z. (2011), Ambient sea noise in the Baltic Sea – review of investigations, *Hydroacoustics*, **14**: 75–82.
11. Klusek Z., Lisimenka A. (2016), Seasonal and diel variability of the underwater noise in the Baltic Sea, *The Journal of the Acoustical Society of America*, **139**(4): 1537–1547, doi: 10.1121/1.4944875.
12. Kochańska I., Nissen I., Marszal J. (2018), A method for testing the wide-sense stationary uncorrelated scattering assumption fulfilment for an underwater acoustic channel, *The Journal of the Acoustical Society of America*, **143**(2): EL116–EL120, doi: 10.1121/1.5023834.
13. Kozaczka E., Grelowska G. (2011), Shipping low frequency noise and its propagation in shallow water, *Acta Physica Polonica A*, **119**(6A): 1009–1012, doi: 10.12693/APhysPolA.119.1009.
14. Mallet A.L. (1975), *Underwater Direction Signal Processing System*, US Patent No 3,870,989.
15. Marage J.P., Mori Y. (2010), *Sonar and Underwater Acoustics*, ISTE Ltd, London UK, and John Wiley & Sons, Inc., NJ, USA.
16. Marszal J., Salamon R., Stepnowski A. (2005), Military sonar upgrading methods developed at Gdansk University of Technology, *Proceedings of the IEEE Oceans'05 Europe Conference*, Brest, France, Vol. 1, pp. 489–494, doi: 10.1109/OCEANSE.2005.1511763.
17. McDonald M.A. (2004), DIFAR hydrophone usage in whale research, *Proceedings of the Acoustics Week in Canada*, **32**(2): 155–160, https://jcaa.caa-aca.ca/index.php/jcaa/article/view/1599.
18. Miller B.S. (2012), Real-time tracking of blue whales using DIFAR sonobuoys, *Proceedings of Acoustics 2012*, Fremantle, Australia, 7 pages.
19. Ren C., Huang Y. (2020), A spatial correlation model for broadband surface noise, *The Journal of the Acoustical Society of America*, **147**(2): EL99–EL105, doi: 10.1121/10.0000710.
20. Roux P., Sabra K.G., Kuperman W.A., Roux A. (2005), Ambient noise cross correlation in free space: Theoretical approach, *The Journal of the Acoustical Society of America*, **117**(1): 79–84, doi: 10.1121/1.1830673.
21. Rudnicki M., Marszal J. (2016), Signal conditioning for examination of shallow-water acoustic noise correlation properties, *Hydroacoustics*, **19**: 335–340.
22. Salamon R. (2004), A directional sonobuoy system for submarine detection, *Hydroacoustics*, **7**: 195–208.
23. Salamon R. (2006), *Sonar systems* [in Polish], Gdanskie Towarzystwo Naukowe, Gdansk, Poland.
24. Salamon R., Marszal J., Raganowicz A., Rudnicki M. (2000), Application of Fourier transformation in a passive sonar with gradient hydrophones, *Proceedings of the Fifth European Conference on Underwater Acoustics ECUA 2000*, Lyon, France 10–13 July 2000; Vol. 2, pp. 1115–1120.
25. Schmidt J.H., Schmidt A., Kochańska I. (2018), Multiple-input multiple-output technique for underwater acoustic communication system, *Proceedings of 2018 Joint Conference – Acoustics, Ustka, Poland, 2018*, IEEE Xplore Digital Library, pp. 280–283. doi: 10.1109/acoustics.2018.8502439.
26. Stover H.A. (1969), *Advanced Direction Finding Sonobuoy System*, US Patent No 3,461,421.
27. Urick R.J. (1983), *Principles of Underwater Sound*, 3rd Ed., Peninsula Pub.
28. Urick R.J. (1986), *Ambient Noise in the Sea*, 2nd Ed., Peninsula Pub.
29. Yang Q., Yang K., Cao R., Duan S. (2018), Spatial vertical directionality and correlation of low-frequency ambient noise in deep ocean direct-arrival zones, *Sensors*, **18**(2): 319, doi: 10.3390/s18020319.
30. Zhou J., Piao S., Huang Y., Zhang S., Qu K. (2017), A spatial correlation model for the horizontal non-isotropic ocean ambient noise vector field, *Journal of Low Frequency Noise, Vibration and Active Control*, **36**(2): 124–137, doi: 10.1177/0263092317711984.